Light Absorption by Brown Carbon over the South-East Atlantic Ocean

Lu Zhang[1], Michal Segal-Rozenhaimer[1,2], Haochi Che[1], Caroline Dang[3,4], Arthur J. Sedlacek III[5], Ernie R. Lewis[5], Amie Dobracki[6], Jenny P.S. Wong[7], Paola Formenti[8], Steven G. Howell[9], Athanasios Nenes[10,11]

5   [1]Department of Geophysics, Tel Aviv University, Tel Aviv, Israel

[2]Bay Area Environmental Research Institute, NASA Ames Research Center, Moffett Field, California, USA

[3]NASA Ames Research Center, Moffett Field, California, USA

[4]Universities Space Research Association, Columbia, Maryland, USA,

[5]Brookhaven National Laboratory, Upton, New York, USA

10   [6]Rosenstiel School of Marine and Atmospheric Science, University of Miami, Miami, USA

[7]Mount Allison University, New Brunswick, CA

[8]Université de Paris and Univ Paris Est Creteil, CNRS, LISA, Paris, France

[9]University of Hawaii at Manoa, Department of Oceanography, Honolulu, USA

[10]Laboratory of Atmospheric Processes and their Impacts, School of Architecture, Civil & Environmental

15   Engineering, École Polytechnique Fédérale de Lausanne, Switzerland

[11]Center for Studies of Air Quality and Climate Change, Institute of Chemical Engineering Sciences, Foundation for 20 Research and Technology Hellas, Greece

Correspondence to: Lu Zhang (luzhang@mail.tau.ac.il)

Abstract. Biomass burning emissions often contain brown carbon (BrC), which represents a large family of light-

20   absorbing organics that are chemically complex and therefore difficult to estimate their absorption of incoming solar radiation, resulting in large uncertainties in the estimation of the global direct radiative effect of aerosols. Here we investigate the contribution of BrC to the total light absorption of biomass burning aerosols over the South-East Atlantic Ocean with different optical models utilizing a suite of airborne measurements from the ORACLES 2018 campaign by introducing an effective refractive index of black carbon (BC), $m_{eBC}=n_{eBC}+ik_{eBC}$,

25   that accounts for all possible absorbing components at 660 nm wavelength to facilitate the attribution of absorption at shorter wavelengths.

Most values of the imaginary part of the refractive index, k_{eBC}, were larger than those commonly used for BC from biomass burning emissions, suggesting contributions from absorbers beyond BC at 660 nm. The TEM-EDX single particle analysis further suggests that these long-wavelength absorbers might include iron oxides, as iron

30   is found to be present only when large values of k_{eBC} are derived. Using this effective BC refractive index, we find that the contribution of BrC to the total absorption at 470 nm ($R_{BrC,470}$) ranges from ~5-15 %, with the organic aerosol mass absorption coefficient ($MAC_{OA,470}$) at this wavelength ranging from 0.25 ± 0.34 m^2 g^{-1} to 0.43 ± 0.12 m^2 g^{-1}. The core-shell model yielded much higher estimates of $MAC_{OA,470}$ and $R_{BrC,470}$ than

homogeneous mixing models, underscoring the importance of model treatment. Another key finding was that estimates of the BrC contribution at 470 nm from the commonly used AAE (absorption Ångström exponent) attribution method (<5%) are much lower than the BrC contribution estimates ($R_{BrC,470}$) using our new methodology that accounts for contributions from both BrC and non-carbonaceous, long-wavelength absorbers,

5 such as magnetite. Thus, it is recommended that application of any optical properties-based attribution method use absorption coefficients at the longest possible wavelength to minimize the influence of BrC at the long wavelength and to account for potential contributions from other absorbing materials.

1 Introduction

Black carbon (BC) and brown carbon (BrC) are two main light-absorbing carbonaceous aerosols that
10 play a significant role in Earth's radiative forcing and climate (Bond et al., 2013; Laskin et al., 2015; Brown et al., 2018). BC is the principal atmospheric particulate absorber that absorbs strongly over the entire solar spectrum (Bond and Bergstrom, 2006). Biomass burning (BB) contributes approximately 2/3 of the global primary organic aerosol (OA) budget, which currently most climate models treat as "white carbon" that only scatters and does not absorb light (Bond et al., 2013). However, studies show that BB OA contains a substantial amount of BrC, which
15 predominantly absorbs at short visible and near-UV wavelengths (Chen and Bond, 2010; Lack et al., 2012; Saleh et al., 2014; Taylor et al., 2020). Feng et al. (2013) found that the absorption of BrC can shift BB direct radiative forcing to positive values. The contribution of BrC to the total absorption by carbonaceous aerosols is estimated to be ~20-50% with a global radiative effect of ~0.03-0.6 W m^{-2} (Kirchstetter and Thatcher, 2012; Wang et al., 2013; Feng et al., 2013; Saleh et al., 2015; Jo et al., 2016). However, values reported by these studies are subject
20 to substantial uncertainties, and investigations of BrC properties are still very much in a developmental stage. Thus, in order to realize a substantive reduction in the uncertainty, better attribution of BrC light absorption must be first accomplished.

To date, several methods have been employed to investigate the light absorption of BrC. The AAE (absorption Ångström exponent) attribution method utilizes the different spectral dependences of the absorption
25 by BC and BrC to determine the contribution from BrC at short wavelengths (Lack and Langridge, 2013; Wang et al., 2018a; Taylor et al., 2020). Most earlier studies assumed the AAE of BC (AAE_{BC}) to be unity, although this assumption may introduce large uncertainties (Lack and Langridge, 2013) because AAE_{BC} varies with size, mixing state, and wavelength (Lack and Cappa, 2010; Fig. 2 in Liu et al., 2015; Liu et al., 2018). Revised methods with more realistic values of AAE_{BC} have been proposed, such as using the AAE from two long-visible
30 wavelengths (Taylor et al., 2020) or that from the Mie model (Wang et al., 2018a). A major drawback of these methods is that they are suitable only for mixtures of BC and BrC, and if other absorbing materials are present, such as dusts, more detailed information is needed to account for their contribution to light absorption at the longer

wavelengths. Another methodology involves measuring the absorption of organics that have been extracted with either an organic solvent or water and represents, thus far, the only way to directly measure BrC absorption (Wong et al., 2019). The drawback to this approach is that not all organics can be extracted with one or two solvents, as highlighted by the work of Chen and Bond (2010), who reported extraction efficiencies of ~70 % in water and

5   ~90 % in methanol. This inability to extract all organics means that insoluble organic substances remain unknown since they are not measured. This, in turn, could lead to cases where the absorption properties of the extracted organics might be different from those derived from in situ measurements. In addition, this method is carried out offline and requires elaborate laboratory analysis. Still another approach to estimate the absorption of BrC is through optical closure, determine the BrC absorption as the difference of the total measured absorption and that

10   of BC calculated using Mie theory (Saleh et al., 2014; Liu et al., 2015). In this approach, the accuracy of BrC absorption relies heavily on the accuracy of BC absorption calculation. Values commonly used for the refractive index of BC (m_{BC}) from BB emissions in these calculations have ranged from 1.5+0.3i to 1.95+0.79i (Liu et al., 2015; Chylek et al., 2019; Taylor et al., 2020), which will lead to large differences in BC absorption simulation results (Taylor et al., 2020). To date there is no consensus on the best value of m_{BC}. Another factor influencing

15   the BC absorption calculation, and hence the estimated BrC absorption, is the mixing state of BC and non-BC components within particles. Liu et al. (2015) used the core-shell (CS) Mie model and Rayleigh-Debye-Gans approximation to investigate the effect of BC microphysics on the estimation of BrC absorption and found it to be highly sensitive to the model treatment. Saleh et al. (2014) compared internal and external mixtures of BC and BrC and found internally mixed cases yielded smaller BrC absorption than externally ones. Similar to the AAE

20   attribution method, the presence of absorbing materials other than BC and BrC can lead to errors in the attribution of BrC absorption. For example, light absorbing FeOx was found to be common in field studies, especially for BB emissions (Ito et al., 2018), yet few studies perform measurements of size distributions and chemical composition by these particle types, making it difficult to separate their contribution to the total absorption from that of BrC.

25   The savannah regions in Africa experience widespread annual BB events from July to October, which are estimated to account to approximately 1/3 of global BB emissions (van der Werf et al., 2010). These aerosols are transported westward over the South-East Atlantic, making this region an ideal natural laboratory for investigating the absorption of BrC from BB emissions. In this study, we estimate the absorption of BrC using the optical closure method utilizing in-situ aircraft measurements and offline single particle analysis from the

30   ORACLES (ObseRvations of Aerosols above CLouds and their intEractionS) 2018 campaign (Redemann et al., 2020). An effective refractive index of BC (m_{eBC}), which attempts to capture the absorption of all possible absorbing components at 660 nm, is introduced to facilitate the absorption attribution at shorter wavelengths. The core-shell model and homogeneous models are applied and compared in this study. The range of values of the

organic aerosol mass absorption coefficient ($MAC_{OA,470}$) and contribution of BrC to the total absorption at 470

nm ($R_{BrC,470}$) using the optical closure method are obtained.

2 Methods

2.1 Site and Instrumentation
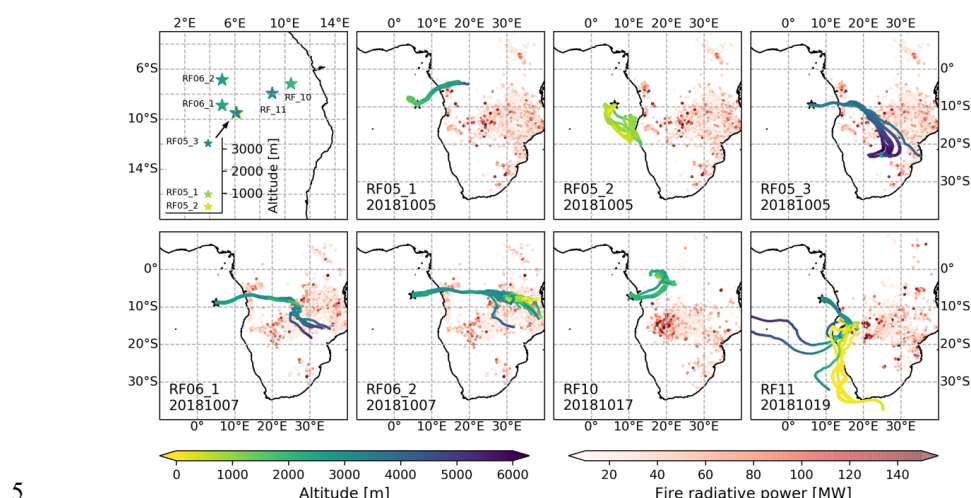
Figure 1: (upper left panel) overview of the flight locations during ORACLES 2018 investigated in this study, and (all other panels) 7-day back trajectories and fire radiative power (FRP) from MODIS 6 Collection Active Fire Detections (MCD14ML) at the end day of the trajectory (only data with confidence >50 % are used here).

ORACLES was a three-year NASA-funded field campaign to investigate the influence of BB emissions from southern Africa on regional and global climate (Redemann et al., 2020). We investigated aerosol optical properties during seven research flights (RF) from the ORACLES 2018 campaign (Fig. 1): RF05_1, RF05_2, RF05_3, RF6_1, RF6_2, RF10, and RF11. The specifications for each flight can be found in Table 1 in Dang et al. (2021). These flights were chosen as they provided investigations of aerosol properties from the marine boundary layer (MBL) and in the free troposphere, from relatively aged aerosols to highly aged aerosols, and are comprehensive in online and offline measurements with few missing data. RF05_1 occurred in mixed cloud and aerosol layer at an altitude of ~1 km, RF05_2 was within the MBL at an altitude of ~380 m, the others were in the aerosol layer above the MBL at an altitude equal to or greater than 2 km. The aging time is taken as the first interception of back trajectories with fires; note this age is strictly minimum age as air can get repeated injections of smoke. The age was estimated to be ~155 h for RF05_1 and ~40 h for RF05_3, RF6_1, RF6_2, RF10, and RF11. The age of RF05_2 was uncertain as its 7-day back trajectories were within the MBL and did not reach the

fires, but based on the result from the Weather Research and Aerosol Aware Microphysics (WRF-AAM) model, it was ~9 h older than RF05_1, and thus the most aged among all samples.

Particle properties measured were non-refractory submicron aerosol composition from an Aerosol Mass Spectrometer (AMS), mass concentrations of refractory BC and mixing state of BC-containing particles from a

5 Single Particle Soot Photometer (SP2), particle number size distribution (PNSD) from an Ultra-High-Sensitivity Aerosol Spectrometer (UHSAS) and Aerodynamic Particle Sizer (APS), light absorption at 470, 530, and 660 nm from a Particle Soot Absorption Photometer (PSAP), light scattering at 450, 550, and 700 nm from a nephelometer (Neph), and particle morphology and elemental composition from filter samples that were analysed by a transmission electron microscopy (TEM) coupled with energy dispersive X-ray (EDX). The light absorption from

10 the PSAP was corrected using the wavelength-average correction scheme following Virkkula (2010) and Pistone et al. (2019). All instruments were mounted in the NASA P-3 aircraft and operated under dry conditions except for the Neph, whose humidity is not controlled. Data for BC mass concentration less than 0.1 μg/m³ or absorption coefficient at 660 nm less than 1.5 Mm⁻¹ were not included. Measurements were averaged to 10 s and adjusted to STP values at 273.15 K and 1013 hPa. More details of the instrumentation are provided in Section S1 of the

15 supplemental information.

2.2 Optical Models

From the TEM images, most of the particles were found to be nearly spherical, with >70% of the particles having aspect ratios <1.5; therefore, we applied Mie theory in our optical simulations. We investigated the sensitivity of our closure simulations to four different models – the ideal core-shell (CS) model and three

20 homogeneous mixing models: 1) the volume mixing (VM) model, 2) the Maxwell-Garnett (MG) model, and 3) the Bruggemann (BG) model. We did not investigate the externally mixing model, as our TEM analysis showed that most of the particles were internally mixed (Dang et al., 2021).

In our optical closure, particles were separated into BC-containing particles and BC-free particles, whose size distributions were calculated with the PNSD of all particles from the UHSAS and APS, and BC 2-D size and

25 mixing state (i.e. coating thickness) distribution of BC-containing particles from the SP2. We applied the aforementioned four models to BC-containing particles. Detailed descriptions and inputs of all four models can be found in Section S2 in the supplement. We assumed that the non-BC components in both populations were homogeneously well mixed and calculated the refractive index of the mixture, $m_{BC\text{-free}}$, with the VM rule, which assumes that the index of refraction of the mixture is the sum of the volume-weighted indices of refraction of the

30 individual components. The mass concentrations of SO_4^{2-}, NO_3^-, NH_4^+, and Cl^- measured by AMS were converted to those of inorganic salts using the simplified ion-pairing scheme proposed by Gysel et al. (2007), modified as follows:

$$n_{NH_4Cl}^{mol} = n_{Cl^-}^{mol} \tag{1}$$

$$n_{NH_4NO_3}^{mol} = \min \left(n_{NO_3^-}^{mol}, n_{NH_4^+}^{mol} - n_{Cl^-}^{mol} \right) \tag{2}$$

$$n_{NH_4HSO_4}^{mol} = \max \left(0, min \left(2n_{SO_4^{2-}}^{mol} - n_{NH_4^+}^{mol} + n_{NO_3^-}^{mol} + n_{Cl^-}^{mol}, n_{NH_4^+}^{mol} - n_{NO_3^-}^{mol} - n_{Cl^-}^{mol} \right) \right) \tag{3}$$

$$n_{(NH_4)_2SO_4}^{mol} = \max \left(0, min \left(n_{SO_4^{2-}}^{mol}, n_{NH_4^+}^{mol} - n_{NO_3^-}^{mol} - n_{Cl^-}^{mol} - n_{SO_4^{2-}}^{mol} \right) \right) \tag{4}$$

$$n_{KNO_3}^{mol} = \max \left(0, min \left(n_{NO_3^-}^{mol}, n_{NH_4^+}^{mol} - n_{NO_3^-}^{mol} - n_{Cl^-}^{mol} - 2n_{SO_4^{2-}}^{mol} \right) \right) \tag{5}$$

$$n_{K2SO_4}^{mol} = \max \left(0, min \left(n_{SO_4^{2-}}^{mol}, n_{SO_4^{2-}}^{mol} - n_{NH_4^+}^{mol} + n_{Cl^-}^{mol} + n_{NO_3^-}^{mol} \right) \right) \tag{6}$$

where n^{mol} represents the number of moles. As potassium salts are the most frequently detected salts from TEM-EDX analysis (Dang et al., 2021), the residual anions were assumed to be combined with potassium, i.e. KNO_3 and K_2SO_4. Note that a small fraction of NO_3^- and SO_4^{2-} detected by AMS might be organic and thus lack an accompanying cation. Densities of the various salts and OA used to convert the mass concentrations to volume concentrations were taken from Kuang et al. (2020; Table 1) and Liu et al. (2015b). Thus, $m_{BC\text{-free}}$ is calculated as

$$m_{BC-free} = \left(\sum_{i=salts} m_i * V_i + m_{OA} * V_{OA} \right) \Big/ \left(\sum_{i=salts} V_i + V_{OA} \right) \tag{7}$$

where m_i and V_i represent the refractive indices and volumes of aforementioned salts; m_{OA} and V_{OA} are those for OA. The refractive indices of salts are taken from Table 1 in Kuang et al. (2020). The quantity $m_{BC\text{-free}}$ is assumed to be the same value for both BC-free particles and the non-BC component in BC-containing particles. The effective refractive indices for the VM, MG, and BG models can then be obtained by the corresponding mixing rules (Section S2 in the supplement). The density of BC is assumed to be 1.8 g cm^{-3} (Bond and Bergstrom, 2006; Liu et al., 2017). The refractive indices of BC and OA will be presented in the following section.

2.3 Optical calculation procedure
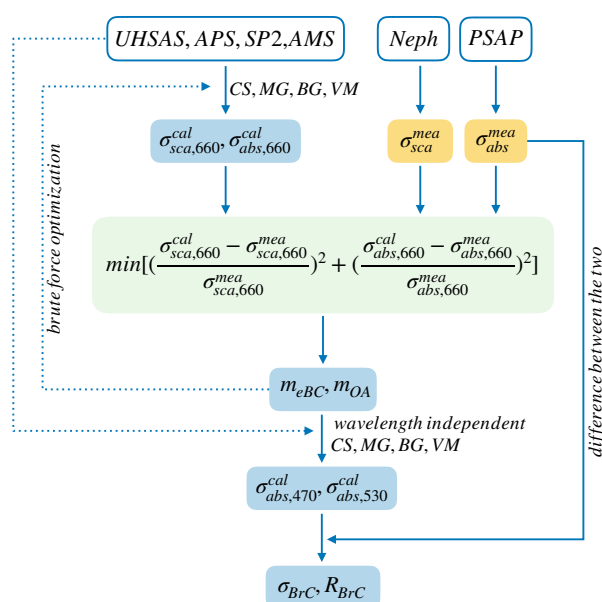
Figure 2: Schematic diagram of the iterative derivation of BrC absorption attribution performed in this study. Cells in white, yellow, and blue represent instrument, measurements, and calculations, respectively. The green box is the optimization step used to determine the values of the effective refractive index of BC, m_{eBC} and the refractive index of OA, m_{OA}, once the deviation of measured and calculated scattering and absorption coefficients at 660 nm are minimized. m_{eBC} and m_{OA} are held constant at investigated wavelengths, i.e. 470, 530, and 660 nm. The imaginary part of the refractive index of OA, k_{OA}, was restricted to 0 in this calculation.
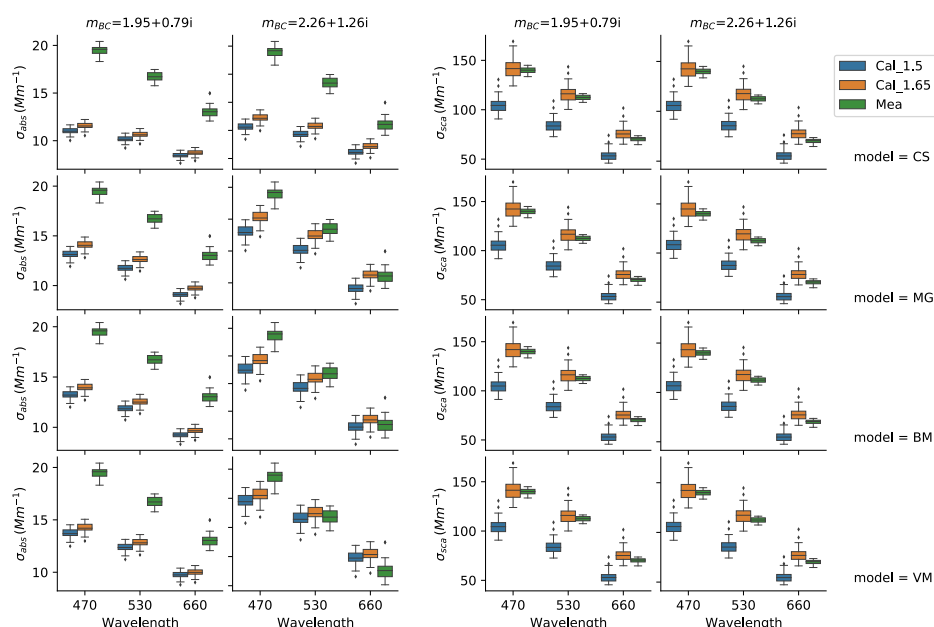
Figure 3: Modelled (blue and orange markers) and measured (green markers) absorption coefficients (σ_{abs}) and scattering coefficients (σ_{sca}) at PSAP wavelengths for RF06_1. Variables are modelled with two commonly used m_{BC} values (shown on the top) and two values of m_{OA} using the CS, MG, BG, and VM models (specified on the right). OA is assumed to be non-absorbing with the refractive index m_{OA} equal to 1.5+0i (blue markers) and 1.65+0i (orange markers), respectively. Values of σ_{sca} measured by the nephelometer at 450, 550, and 700 nm are interpolated to PSAP wavelengths, 470, 530, and 660 nm using the scattering Ångström exponent (Section S3 in the supplement).

We introduce an effective refractive index of BC, m_{eBC}, to represent the refractive index of BC and any other absorbing components **at 660 nm** in this study. The m_{eBC} is defined as $m_{eBC} = n_{eBC}+ik_{eBC}$, where n_{eBC} and k_{eBC} are the real and imaginary parts of m_{eBC}, respectively. The m_{eBC} is proposed based on three considerations. Firstly, the numerical value selected for m_{BC} has a large impact on the absorption attributed to BC (Fig. 3 and Fig. S3), and hence on the estimated absorption by BrC, but as note above, there is no consensus on the best value of m_{BC} yet. Secondly, the lack of measurements of possible absorbers other than BC and BrC such as magnetite makes it difficult to correctly estimate the BrC absorption, so approaches that take these components into consideration are required. Thirdly, aged BrC is usually considered to be non-absorbing at long visible wavelengths (Chen and Bond, 2010; Lack et al., 2012), thus we assume m_{eBC} does not include the absorptivity of BrC and therefore the BrC absorption can be differentiated from absorption from other substances. This assumption has not considered tar balls, which are ubiquitous in fresh plumes and absorbing at infrared

wavelengths; considering the aging time of our samples, the absorption of tar balls is expected to be small or negligible (Sedlacek III et al., 2018; Adler et al., 2019; Li et al., 2019).

The m_{eBC} is named the effective refractive index of BC as it is supposed to be contributed mainly or entirely by BC. The m_{eBC} would be the same as m_{BC} if the absorption at 660 nm is solely contributed by BC;

5 however, if other absorbing components are present, the imaginary part (k_{eBC}) of m_{eBC} would be greater than that (k_{BC}) of m_{BC}, the amount of which depends on the absorptivity and relative amount of these absorbers. The retrieval of m_{eBC} is illustrated in Fig. 2; the real refractive index of OA (n_{OA}) is retrieved as well because it has an impact, albeit small, on the BC absorption calculation (Fig. 3 and Fig. S3). Note that OA is assumed to be non-absorbing with the imaginary refractive index $k_{OA}=0$ in the whole calculation. We determined the values of m_{eBC} and m_{OA}

10 by minimizing the sums of the squares of the relative differences between the measured and calculated scattering and absorption coefficients at 660 nm for each of the four models:

$$\chi^2(m_{eBC}, m_{OA}) = (\frac{\sigma_{sca,660}^{cal} - \sigma_{sca,660}^{mea}}{\sigma_{sca,660}^{mea}})^2 + (\frac{\sigma_{abs,660}^{cal} - \sigma_{abs,660}^{mea}}{\sigma_{abs,660}^{mea}})^2 \qquad (8)$$

Values of n_{eBC}, k_{eBC} and n_{OA} are varied from 1.5 to 4, 0.3 to 2.5 (Chylek et al., 2019; Taylor et al., 2020) and 1.35 to 1.7 (Lack and Cappa, 2010; Liu et al., 2013; Saleh et al., 2014; Moise et al., 2015), respectively – over greater range than those recorded in literature. Values of χ^2/N greater than 10% are excluded, where N stands for the

15 total data number. The quantities $\sigma_{abs,660}^{cal}$ and $\sigma_{abs,660}^{mea}$ are the calculated and measured absorption coefficients at 660 nm, respectively, and $\sigma_{sca,660}^{cal}$ and $\sigma_{sca,660}^{mea}$ are the calculated and measured scattering coefficients at 660 nm, respectively, where $\sigma_{sca,660}^{mea}$ is determined by interpolated using the scattering Ångström exponent from scattering coefficients measured by the nephelometer (Section S3 in the supplement). Only absorption is used in the calculation of χ^2 for RF05_1 and RF05_2, as measured and simulated scattering coefficients are not comparable

20 (discussed in detail in Section S1.2 in the supplement):

$$\chi^2(m_{eBC}, m_{OA}) = \sum_{\lambda=660} (\frac{\sigma_{abs,\lambda}^{cal} - \sigma_{abs,\lambda}^{mea}}{\sigma_{abs,\lambda}^{mea}})^2 \qquad (9)$$

We assume the m_{eBC} and m_{OA} remain constant over the range of investigated wavelengths, i.e. 470-660 nm, and calculate the absorption coefficients at 470 and 530 nm ($\sigma_{abs,470}^{cal}$ and $\sigma_{abs,530}^{cal}$) for each flight using the different models. The values of m_{BC} and m_{OA} are usually considered to be very weakly dependent on, or independent of, wavelength in the visible spectrum (e.g., Chang and Charalampopoulos, 1990; Moteki et al., 2010;

25 Saleh et al., 2014). As will be discussed later in Section 3.1, absorbers that contribute to m_{eBC} besides BC are mainly regarded as magnetite, whose refractive index is generally invariant between wavelengths 470 and 660 nm. Thus, the assumption of constant m_{eBC} and m_{OA} between 470 and 660 nm is reasonable in our study, although it may lead to underestimations of BrC absorption for highly aged particles, as discussed further in Section 3.2. In addition, the absorption by BrC may be slightly underestimated without incorporating tar balls into the

30 calculation. As illustrated in Fig. 2, the absorption at shorter wavelengths is assumed to be determined by that

from BrC, and that from all other absorbing components, the latter of which is characterized entirely by m_{eBC}. Therefore, the absorption of BrC at wavelength λ ($\sigma_{abs,BrC,\lambda}$) can be calculated as the difference between measured absorption coefficients ($\sigma_{abs,\lambda}^{mea}$) and the ones calculated with m_{eBC} ($\sigma_{abs,\lambda}^{cal}$):

$$\sigma_{abs,BrC,\lambda} = \sigma_{abs,\lambda}^{mea} - \sigma_{abs,\lambda}^{cal} \qquad (10)$$

The quantity $R_{BrC,\lambda}$, defined as

$$R_{BrC,\lambda} = \sigma_{abs,BrC,\lambda}/\sigma_{abs,\lambda}^{mea} \qquad (11)$$

5 is the fractional contribution of BrC to the total absorption at wavelength λ, which is assumed to be zero at 660 nm in our study. The mass absorption coefficient (MAC) of OA ($MAC_{OA,\lambda}$) at wavelength λ can be determined from $\sigma_{abs,BrC,\lambda}$ and the mass concentration of OA, M_{OA}, as:

$$MAC_{OA,\lambda} = \sigma_{abs,BrC,\lambda}/M_{OA} \qquad (12)$$

Similarly, the mass absorption coefficient of BC (MAC_{BC}) is defined as: $MAC_{BC} = \sigma_{abs}^{mea}/M_{BC}$, where σ_{abs}^{mea} and M_{BC} represent the measured absorption coefficient and the mass concentration of BC.

10 **3 Results and discussion**

3.1 Effective refractive index of BC (m_{eBC})

In this section, we present and discuss the results of m_{eBC} derived from the aforementioned four models using the AMS, SP2, APS, and UHSAS data for each sample. The values of k_{eBC} for each sample determined by the various models are shown in Figure 4. Also shown in that figure is the mass ratio (MR) of non-BC to BC

15 substance for BC-containing particles, calculated as $MR = \frac{\sum_i (D_{p,i}^3 - D_{c,i}^3)*\rho_{BC-free}}{\sum_i D_{c,i}^3*\rho_{BC}}$, where D_p and D_c are diameters of coated BC particles and mass-equivalent diameters of BC core, respectively. The MR_{100} is the MR for particles with 100 nm BC core only, i.e. D_c equals to 100 nm. As stated in Section 2.3, values of m_{eBC} for RF05_1 and RF05_2 are constrained only by absorption coefficients with Eq. 9. To justify its feasibility, we derived m_{eBC} for other flights using Eq. 9 and found the differences are less than 5% for both the real and imaginary parts. No result

20 for RF05_3 was obtained with CS model because no m_{eBC} value has been achieved in the retrieval.

The variation of k_{eBC} shows a similar pattern among different models (Fig. 4). Those values derived from the CS and VM models are the highest and lowest, respectively, consistent with modelling results for absorption in previous studies (e.g. Taylor et al. 2020), and those from the MG and BG models are between the other two and are very close to each other. The values of k_{eBC} for RF05_1, RF05_2, RF06_1, and RF06_2 from the CS

25 model have greatly exceeded the largest k_{BC} of commonly used values of m_{eBC} (grey shaded region in Fig. 4), determined by Moteki et al. (2010) for soot particles from an urban source, Tokyo. Except for RF10, little confidence can be placed in the value of k_{eBC} from the CS model, for two main reasons. First, the bulk MR for all samples is less than 2, and application of the CS model may be inappropriate for particles with such low MR values (Liu et al., 2017). Second, the TEM analysis found few core-shell structures (e.g., example of RF05_1 in

Fig. 5) among all investigated samples, with most BC-containing particles composed of condensed BC nodules internally mixed with salts/organics (e.g., example of RF05_3 in Fig. 5) or aggregates attached to non-BC components (e.g., example of RF05_2 in Fig. 5). Figure 5 shows representative TEM images of different types of BC-containing particles for each flight. Although a fair number of BC particles homogeneously mixed with salts

5   and OA were detected from TEM for RF10 (Fig. 5), which seems to resemble homogeneous models, this sample is thickly coated, with MR equal to 7.4 and MR_{100} equal to 22.5, largely exceeded the threshold value of MR for the CS model specified in Liu et al. (2017). In addition, results of BrC contribution to the total absorption also suggest that the CS model for RF10 is more reasonable, which will be discussed in detail in Section 3.3.
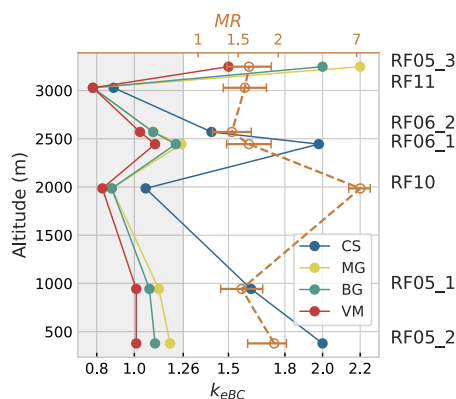
10   **Figure 4: Values of k_{eBC} (closed dots) derived from different models and MR (orange open dots, top x-axis) for each flight. Error bars of MR represent 17% uncertainty. The top x-axis is using the log scale. Grey shaded region for k_{eBC} < 1.26 marks the range of values of k_{BC} commonly used for BC.**
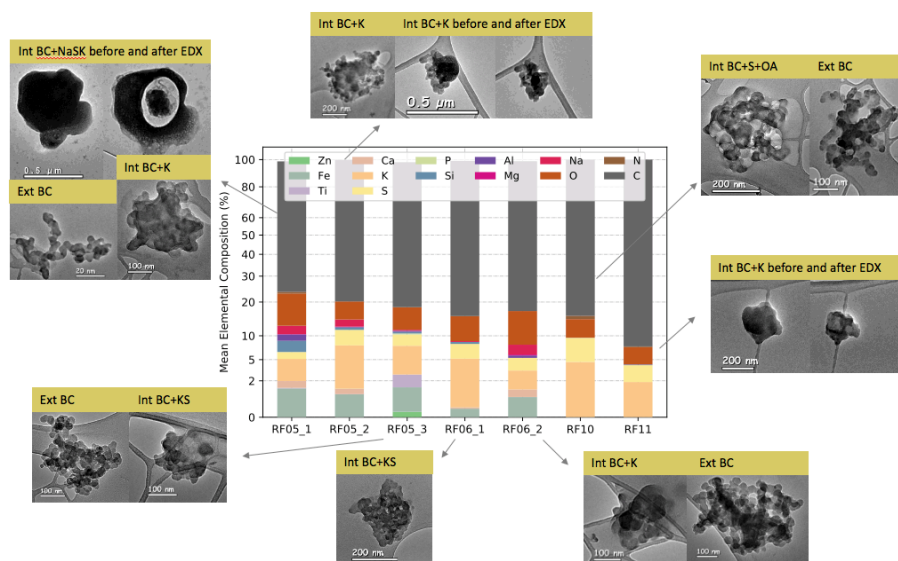
Figure 5: Elemental composition and representative microphysical images of different types of BC-containing particles from TEM analysis for each flight. Int BC and Ext BC represent internally and externally mixed BC particles, respectively. For example, Int BC+K stands for internally mixed BC with potassium salts. The y-axis uses a $x^{1/2}$ scale.

As discussed in section 2.3, m_{eBC} should be the same as m_{BC} if the absorption at 660 nm arises only from BC; otherwise, higher k_{eBC} values indicate larger contributions of absorbers other than BC at 660 nm. The values of k_{eBC} for RF05_1, RF05_2, RF05_3, RF06_1, and RF06_2, for which iron (Fe) was detected from the TEM-EDX (as shown in the bar chart in Fig. 5), are greater than those for RF10 and RF11, for which no iron was detected. Therefore, we suspect higher k_{eBC} values are related to iron oxides (FeOx) that absorbs at 660 nm, which we suspect to be magnetite, based on the following three points. Firstly, magnetite absorbs strongly and uniformly over the visible spectrum with the imaginary refractive index ranging from 0.58 to 1.0 according to literature (Amaury et al., unpublished data, http://www.astro.uni-jena.de/Laboratory/OCDB/mgfeoxides.html; Ackerman and Toon, 1981; Zhang et al., 2015), and can thereby contribute to the high values of k_{eBC} at 660 nm. Secondly, magnetite can be transformed at high temperatures from Fe(III), such as goethite and hematite (Till et al., 2015; Ito et al., 2018), which happen to be the two most abundant forms of FeOx in African dust (Formenti et al., 2014). Therefore, it is speculated that a part of the magnetite is converted from Fe(III) during biomass burning. Thirdly, magnetite can be emitted by anthropogenic combustion, such as steel manufacturing, oil combustion, and vehicle emissions (Liati et al., 2015; Ito et al., 2018; Kurisu et al., 2019). Its significance in radiative forcing and carbon cycle has been investigated and highlighted in recent studies (Moteki et al., 2017; Ito et al., 2018; Lamb et al., 2021). Although there is no study on pyrogenic iron in sub-Saharan Africa yet, we speculate that anthropogenic combustion emissions in Africa, especially in coastal areas, may also contribute magnetite.

Among all flights, RF05_3, collected at the uppermost aerosol layer (Fig. 4), is an exception, since the values of the absorption coefficient at 660 nm calculated with all four models are considerably smaller than the measured ones (Fig. S3). The MG, BG, and VM models yield k_{eBC} values greater than 1.5, and no value was attained with the CS model. The MAC_{BC} of RF05_3 is the highest among all those investigated with values of

5   20.0 ± 0.8, 17.8 ± 0.8, and 14.3 ± 0.7 m^2 g^{-1} at 470, 530, and 660 nm, respectively. The absorption enhancement, E_{Abs}, defined as the ratio of MAC_{BC} to the value for uncoated BC reported by Bond and Bergstrom (2006), is 2.3 ± 0.1 for all three wavelengths. To the best of our knowledge, except for modelling or laboratory studies of thickly coated particles (Bond et al., 2006; Jacobson, 2012; Peng et al., 2016), such high values of E_{Abs}, particularly at long visible wavelengths, are rarely reported in field measurements (Cui et al., 2016). Taylor et al. (2020)

10 presented relatively high MAC_{BC} values of 20 ± 4, 15 ± 3, and 12 ± 2 m^2 g^{-1} at 405, 514, and 655 nm, respectively and an E_{Abs} of 1.85 ± 0.45 for the CLARIFY 2017; however, these values are still smaller than those for RF05_3. Particles in CLARIFY 2017 are universally thickly coated, with median MR values of 8-12, and are therefore believed to have a largely enhanced lensing effect, which is not the case for RF05_3, which for which MR (Fig. 4) was equal to 1.6 and MR$_{100}$ was equal to 5.3. The calculated absorption coefficient for RF05_3 at 660 nm,

15 using m_{BC} of $1.95+0.79i$ and m_{OA} of $1.65+0i$, was only 59% of the measured absorption coefficient (Fig. S3), implying that the remaining 41% of absorption was contributed by other absorbers. This huge absorption from other absorbers in this flight may indicate a much larger amount of magnetite compared to other flights. In addition, we noticed titanium (Ti) on the particles analyzed from RF05_3. Formenti et al. (2014) found the mineral dust in western Africa consists mainly of clays, quartz, iron, and titanium oxides, which together represent at least 92%

20 of the dust mass. Although titanium oxides are not absorbing, several forms of Ti have been reported to strongly absorb at visible wavelengths (Pflüger and Fink, 1997; Palm et al., 2018). Therefore, we suspect this large absorption may also be related to absorbing titanium compounds.

3.2 Mass absorption coefficient of OA (MAC$_{OA}$)
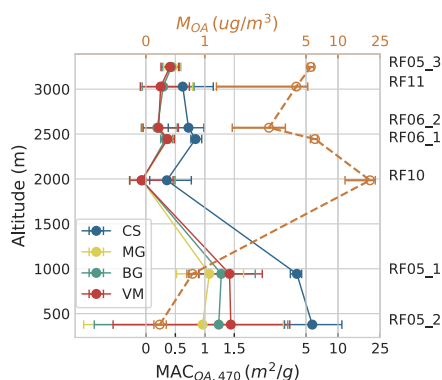
Figure 6: Values of $MAC_{OA,470}$ (closed dots) derived using different models and mass concentrations of OA, M_{OA} (orange open dots, top x-axis), for each flight. Error bars represent the 10th and 90th percentile. The scale of both x-axes is symmetric log.

Values of $MAC_{OA,470}$ calculated from Eq. 12 using the different models are shown in Fig. 6. The values

5 of $MAC_{OA,470}$ from the three homogeneous models were fairly close to each other; while $MAC_{OA,470}$ from the CS model was much greater, highlighting the importance of the proper model treatment. From Section 3.1, results of RF10 from the CS model, and other flights from homogeneous models, are more plausible, with values of $MAC_{OA,470}$ for RF05_3, RF06_1, RF06_2, RF10, and RF11 ranging from 0.25 ± 0.34 m^2/g to 0.43 ± 0.12 m^2/g. Our result at 470 nm is slightly lower or generally comparable to the value 0.31 ± 0.09 m^2/g at 405 nm for highly aged

10 aerosols sampled downwind of ORACLES in CLARIFY 2017 campaign (Taylor et al., 2020), suggesting BrC bleaching during transport considering our result is at a much longer wavelength (Che et al., 2021).

RF05_1 and RF05_2, whose particles are equally or even more aged than those in CLARIFY, showed unexpectedly high $MAC_{OA,470}$ values of 1.18 ± 0.54 m^2/g and 1.07 ± 1.60 m^2/g, respectively. Although M_{OA} for these samples are low (Fig. 6), measurements from all instruments are within the detection limit, which would argue

15 that the values are valid. Wang et al. (2018) used airborne measurements to constrain their global model and found the best MAC_{OA} to represent the measurements is 1.33 m^2/g for freshly emitted BB OA at 365 nm. Lin et al. (2017) investigated relatively fresh BB aerosols subject to atmospheric processes during a night-long BB event in an urban environment and got a MAC of 0.9 m^2/g for water extractable BrC at 470 nm under the peak BB episode. Our values of $MAC_{OA,470}$ for RF05_1 and RF05_2 are higher than those for much fresher BB aerosols, which

20 seems unrealistic, as BrC bleaching is expected to occur during transport. One possible explanation is that secondary BrC formation occurred, perhaps through aqueous-phase chemistry during transport (Hems et al., 2021), for RF05_1 and RF05_2, which were sampled in or close to the MBL with higher RHs. Saleh et al. (2013) reported that secondary BrC can be more absorbing than primary BrC at short visible wavelengths; however, to the best of our knowledge, such high MAC for secondary BrC have not been documented (Kasthuriarachchi et al., 2020).

25 As we assume a constant m_{eBC} over the investigated spectrum, i.e. 470-660 nm, if there are some components with strong absorption at short visible but not at long visible wavelengths, the m_{eBC} would be underestimated at shorter wavelengths and therefore MAC_{OA} would be overestimated. Hematite, whose imaginary refractive index ranges from 0 to 1.0 at 470 nm and 0 to 0.4 at 670 nm (Zhang et al., 2015; Go et al., 2021), is the second most abundant FeOx in western African dust (Formenti et al., 2014). Particles in RF05_1 and RF05_2

30 experienced approximately 6 days of transport and thus may have had more opportunities to mix with hematite and therefore lead to an overestimation of MAC_{OA}. While lacking measurements on these absorbers, it is difficult to verify our speculation. A modified SP2 has been reported by (Yoshida et al., 2016) that can discriminate black-

coloured magnetite and red-coloured hematite; thus, we recommend adding such measurements in BB investigations.

3.3 Contribution of BrC to total absorption (R_{BrC})
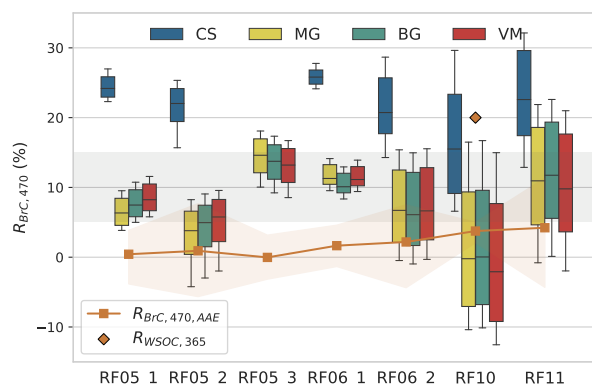
5   **Figure 7: Contribution of BrC to the total absorption obtained from optical closure approach in this study (boxes, $R_{BrC,470}$) and from the AAE attribution method (orange squares, $R_{BrC,470,AAE}$) at 470 nm. The grey zone indicates the $R_{BrC,470}$ range of 5-15% in this study. Orange shades of $R_{BrC,470,AAE}$ represent the 10th and 90th percentile. The orange diamond is the contribution of WSOC to the total absorption, $R_{WSOC,365}$ (personal communication).**

Attribution (%)	470 nm	530 nm	660 nm
BrC	11	4	0
Other absorbers	18	21	36
BC	71	75	74
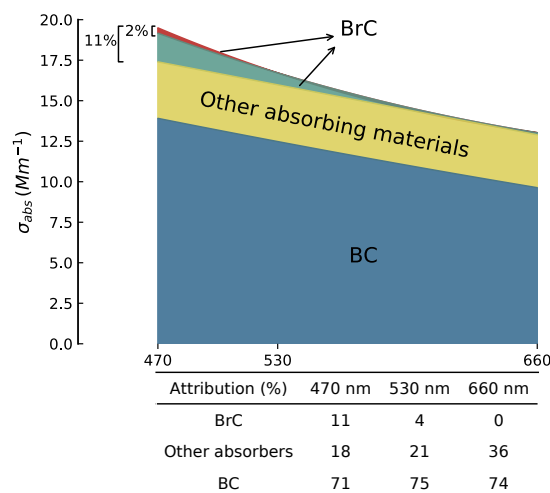
10   **Figure 8: Illustration of the attribution of absorption for RF06_1. Blue area represents the absorption of BC, calculated with m_{BC}=1.95+0.79i and m_{OA}=1.65+0i using BG model. The upper border of the yellow region represents absorption coefficients calculated with corresponding m_{eBC} and m_{OA} for RF06_1 using BG model assuming non-absorbing OA; the yellow area illustrates the absorption by absorbing components besides BC and BrC, calculated as the difference**

between the two absorption coefficients calculated by the BG model using m_{eBC} and m_{BC}, respectively. The upper border of the red region is drawn with measured absorption coefficients at 470, 530, and 660 nm. The red region stands for the BrC absorption coefficient calculated from the AAE attribution method with Eq. 14. The 2% and 11% are the proportions of BrC at 470 nm estimated from the AAE attribution method and our optical closure method, respectively.

5   The table in the lower panel shows the absorption attribution at 470, 530, and 660 nm from the optical closure method.

The contribution of BrC to the total absorption at 470 nm, $R_{BrC,470}$, which was calculated using the optical closure method from Eq. 11, is shown in Fig. 7. Similar to the results for MAC$_{OA}$, the MG, BG, and VM models yield fairly close results for $R_{BrC,470}$, while those from the CS model are higher. It is noted that the values of $R_{BrC,470}$ from MG, BG, and VM models at 470 nm for RF10 are near zero, which is unrealistic for the following three

10   reasons. Firstly, RF10 was sampled after approximately 40 hours of transport; although there are considerable photobleaching and oxidative whitening of BrC when removed from its source for a day or more, it is unlikely that BrC will be completely bleached with a 40 h aging time (Hems et al., 2021). Secondly, samples in this study with similar aging times, i.e. RF05_3, RF06_1, RF06_2, and RF11, all showed a much greater contribution of BrC to absorption. Finally, Nenes et al. (personal communication) reported the contribution of water-soluble BrC

15   to the total absorption at 365 nm of 20%. As our RF10 was measured 10 min earlier at a similar location in the plume and no distinct changes were observed in either the meteorological conditions or aerosol properties, we expect the AAE of BrC derived from these two results to be within the range of those from literature. Since the absorption coefficient of BrC at 365 nm is unknown, we assumed it to be 20% of the measured absorption coefficient at 470 nm and calculated the AAE of BrC between 365 and 470 nm with the calculated BrC absorption

20   coefficient at 470 nm from homogeneous models. This AAE is much lower than the actual AAE for BrC as the BrC absorption coefficient at 365 nm is greatly underestimated, but it is still well above the upper limit of the AAE range, ~2-11, reported in the literature (Laskin et al., 2015). As discussed in Section 3.1, the values of $R_{BrC,470}$ for RF10 from the CS model and RF05_1, RF05_2, RF05_3, RF06_1, RF06_2, and RF11 from homogeneous models are more plausible than those from the CS model. As discussed in Section 3.2, particles of RF05_1 and

25   RF05_2 may contain hematite, in which cases their $R_{BrC,470}$ may have been overestimated. Generally, in our study, the $R_{BrC,470}$ ranges from ~5-15 % at 470 nm (grey zone in Fig. 7). This value is lower than the contribution of 13-26 % at 500 nm for relatively fresh OA in the wood smoke from Kirchstetter and Thatcher (2012). Comparing to the result of ~11 % at 405 nm for highly aged aerosols from CLARIFY 2017, which were sampled downwind of ORACLES with 4-8 d aging time, our result is generally comparable while under a much longer wavelength,

30   implying the bleaching of BrC during transport (Taylor et al., 2020; Che et al., 2021).

We calculated the contribution of BrC to the total absorption using the AAE attribution method ($R_{BrC,470,AAE}$) and compared it with that from our optical closure method ($R_{BrC,470}$). In the AAE attribution method, the absorption coefficient of BC at the investigated wavelength (470 nm in our case) is determined by

extrapolating the absorption coefficient at a longer wavelength (530 nm in our case) with the AAE of BC. For example, in this study, the average AAE at 530/660 wavelength pair ($AAE_{530/660}$) for all flights is 0.93±0.16, within the range expected for BC. Thus, we assume that the absorption coefficients at 530 nm ($\sigma_{abs,530}^{mea}$) and $AAE_{530/660}$ have no significant contribution from BrC and that the AAE for BC is independent of wavelength. The

5   contribution of BrC to the total absorption, $R_{BrC,470,AAE}$, can then be calculated in below.

$$R_{BrC,470,AAE} = 1 - \frac{\sigma_{abs,470}^{cal,AAE}}{\sigma_{abs,470}^{mea}} \tag{13}$$

$$\sigma_{abs,470}^{cal,AAE} = \sigma_{abs,530}^{mea}\left(\frac{530}{470}\right)^{AAE_{530/660}} \tag{14}$$

$$AAE_{530/660} = -\frac{\ln(\sigma_{abs,530}^{mea}/\sigma_{abs,660}^{mea})}{\ln(530/660)} \tag{15}$$

$\sigma_{abs,470}^{mea}$, $\sigma_{abs,530}^{mea}$, and $\sigma_{abs,660}^{mea}$ represent the measured absorption coefficients at 470, 530, and 660 nm, respectively. $\sigma_{abs,470}^{cal,AAE}$ is the absorption coefficient calculated from the AAE attribution method at 470 nm. Actually, this assumption is not always true as the AAE varies with both the wavelength and core size and coating thickness of BC particles (Lack and Cappa, 2010; Wang et al., 2016). The results of $R_{BrC,470,AAE}$ are shown in Fig.

10   7, with averages of all flights below 5%, roughly a factor of three smaller than $R_{BrC,470}$.

       The extreme underestimation from the AAE attribution method is mainly due to the fact that the AAE and absorption coefficients used in this method are not derived from BC alone, but include contributions from other absorbing substances. Take RF06_1 as an example, the contribution of BrC derived from the AAE attribution method is 2%, approximately a factor of five smaller than that from our optical closure method with

15   the BG model, 11% (Fig. 7 and 8). As illustrated in Fig. 8, the absorption coefficient at 530 nm used in Eq. 14 and 15 includes the contribution of BrC, which accounts for 4% of the total absorption, and that of absorbers beyond BC and BrC, which accounts for 21%. Note this attribution is based on the BC absorption coefficient calculated from the BG model with m_{BC}=1.95+0.79i, which will vary with the value of m_{BC}. If we remove the 4% BrC from $\sigma_{abs,530}^{mea}$ in Eq. 14, the contribution would increase to 6%, two times larger than 2%, indicating that even

20   though BrC may exist as a small portion at the long wavelength, its impact on the AAE attribution method can be substantial. Thus, we recommend that application of any optical properties-based attribution method to use absorption coefficients at the longest possible wavelength to minimize the influence of BrC, and in the meanwhile, to account for potential contributions from other absorbing materials.

4 Conclusions

25   We investigated the contribution of BrC to the total absorption with different models utilizing measurements from ORACLES 2018 field campaign. An effective BC refractive index, m_{eBC}=n_{eBC}+ik_{eBC}, that was constrained by scattering and absorption measurements to account for all absorbing components at 660 nm, was introduced in this study. Most of the values derived for k_{eBC} were greater than the commonly used k_{BC} values,

suggesting contributions from absorbing materials besides BC at 660 nm. TEM-EDX single particle analysis further suggests that these absorbers might include FeOx that absorbs at long visible wavelengths, i.e. magnetite, as Fe is only present for flights with large values of k_{eBC}. RF05_3 yielded the largest values of k_{eBC}, approximately 40% -140% greater than that of other flights, implying a greater contribution of absorbers besides BC to the total

5 absorption at 660 nm than other flights, which could be due to a larger amount of magnetite in these samples or the result of possible absorbing titanium compounds, which are present on this filter.

As refractive indices of BC and magnetite are generally constant over the range of wavelengths considered, i.e. 470 and 660 nm, we assumed m_{eBC} to be independent of wavelength and calculated MAC_{OA} and the contribution of BrC to total absorption at 470 nm, $R_{BrC,470}$, using different models. The values of $MAC_{OA.470}$

10 and $R_{BrC,470}$ from the three homogeneous mixing models were fairly close to each other, while those from the CS model were much higher, underscoring the importance of proper model treatment. The values of $MAC_{OA.470}$ and contribution of BrC to the total absorption, $R_{BrC,470}$, from the CS model for RF10 and homogeneous models for other flights are found to be more plausible, based on the morphology from TEM images, MR values from SP2, and the validation of the WSOC results. The values of $R_{BrC,470}$ ranged from ~5-15 %, with $MAC_{OA.470}$ varying

15 between 0.25±0.34 m^2 g^{-1} and 0.43±0.12 m^2 g^{-1} for the various flights. Values from our results were generally comparable with MAC_{OA} of 0.31±0.09 m^2 g^{-1} and R_{BrC} of ~11 % at 405 nm for highly aged aerosols from CLARIFY 2017, which were sampled downwind of ORACLES with 4-8 d aging time, while under a much longer wavelength, i.e. 470 nm, implying the bleaching of BrC during transport. High $MAC_{OA,470}$ values of 1.18±0.54 and 1.07±1.60 m^2 g^{-1} were observed for RF05_1 and RF05_2, respectively, which is suspected to be due to the

20 presence of hematite, an abundant FeOx in African dust, which may have mixed with the BC particles during the ~6 d transport. Measurements of a modified SP2 that can distinguish between hematite and magnetite and obtain FeOx concentrations is highly recommended.

Contribution of BrC to the total absorption obtained from the AAE attribution method, $R_{BrC,470,AAE}$, were calculated and compared to that from our optical closure method. $R_{BrC,470,AAE}$ is generally <5%, approximately a

25 factor of three smaller than those from our optical closure method. From the absorption attribution of RF06_1 as an example, we found this underestimation is mainly due to the influence of absorbers besides BC in parameters used in this approach. Thus, when applying optical properties-based attribution methods, it is recommended to use the absorption coefficient at the longest possible wavelength to minimise the influence of BrC and to account for other absorbers in the meanwhile.

30

Acknowledgements. The authors would like to thank the ORACLES team and the postdoctoral fellowship funding from Tel Aviv University, Department of Exact Sciences. Arthur J. Sedlacek III and Ernie R. Lewis thank the Scientific Focus Area (SFA) Science Plan program that is supported by the Office of Biological and

Environmental Research in the Department of Energy, Office of Science, through the United States Department of Energy Contract No. DE-SC0012704 to Brookhaven National Laboratory.

Data availability. Airborne measurements are available via the digital object identifier provided under ORACLES

5 Science Team reference: https://doi.org/10.5067/Suborbital/ORACLES/P3/2018_V2.

Author contributions. MSR and LZ developed the ideas for the direction of the paper. MSR, AJS, EL, AD, JPW, PF, SGH, and AN carried out the airborne measurements. MSR, HC, CD, AJS, EL, AD, JPW, SGH, and AN processed the aircraft data. LZ and HC performed the data analysis. LZ prepared the paper with inputs and

10 comments from all co-authors.

Competing interests. The author declares that there is no conflict of interest.

Special issue statement. This article is part of the special issue "New observations and related modeling studies

15 of the aerosol-cloud-climate system in the Southeast Atlantic and southern Africa regions (ACP/AMT inter-journal SI)". It is not associated with a conference.

References

Ackerman, T. P. and Toon, O. B.: Absorption of visible radiation in atmosphere containing mixtures of absorbing and nonabsorbing particles, Appl. Opt., 20, 3661–3668, https://doi.org/10.1364/AO.20.003661, 1981.

20 Adler, G., Wagner, N. L., Lamb, K. D., Manfred, K. M., Schwarz, J. P., Franchin, A., Middlebrook, A. M., Washenfelder, R. A., Womack, C. C., Yokelson, R. J., and Murphy, D. M.: Evidence in biomass burning smoke for a light-absorbing aerosol with properties intermediate between brown and black carbon, Aerosol Sci. Technol., 53, 976–989, https://doi.org/10.1080/02786826.2019.1617832, 2019.

Bond, T. C. and Bergstrom, R. W.: Light Absorption by Carbonaceous Particles: An Investigative Review,
25 Aerosol Sci. Technol., 40, 27–67, https://doi.org/10.1080/02786820500421521, 2006.

Bond, T. C., Habib, G., and Bergstrom, R. W.: Limitations in the enhancement of visible light absorption due to mixing state, J. Geophys. Res. Atmospheres, 111, https://doi.org/10.1029/2006JD007315, 2006.

Bond, T. C., Doherty, S. J., Fahey, D. W., Forster, P. M., Berntsen, T., DeAngelo, B. J., Flanner, M. G., Ghan, S., Kärcher, B., Koch, D., Kinne, S., Kondo, Y., Quinn, P. K., Sarofim, M. C., Schultz, M. G., Schulz, M.,
30 Venkataraman, C., Zhang, H., Zhang, S., Bellouin, N., Guttikunda, S. K., Hopke, P. K., Jacobson, M. Z., Kaiser, J. W., Klimont, Z., Lohmann, U., Schwarz, J. P., Shindell, D., Storelvmo, T., Warren, S. G., and Zender, C. S.:

Bounding the role of black carbon in the climate system: A scientific assessment, J. Geophys. Res. Atmospheres, 118, 5380–5552, https://doi.org/10.1002/jgrd.50171, 2013.

Brown, H., Liu, X., Feng, Y., Jiang, Y., Wu, M., Lu, Z., Wu, C., Murphy, S., and Pokhrel, R.: Radiative effect and climate impacts of brown carbon with the Community Atmosphere Model (CAM5), Atmospheric Chem.

5   Phys., 18, 17745–17768, https://doi.org/10.5194/acp-18-17745-2018, 2018.

Che, H., Segal-Rozenhaimer, M., Zhang, L., and Dang, C.: Transport and aging of biomass burning aerosols in the South-eastern Atlantic Ocean, Commun. Earth Environ., Under review, 2021.

Chen, Y. and Bond, T. C.: Light absorption by organic carbon from wood combustion, Atmospheric Chem. Phys., 10, 1773–1787, https://doi.org/10.5194/acp-10-1773-2010, 2010.

10   Chylek, P., Lee, J. E., Romonosky, D. E., Gallo, F., Lou, S., Shrivastava, M., Carrico, C. M., Aiken, A. C., and Dubey, M. K.: Mie Scattering Captures Observed Optical Properties of Ambient Biomass Burning Plumes Assuming Uniform Black, Brown, and Organic Carbon Mixtures, J. Geophys. Res. Atmospheres, 124, 11406–11427, https://doi.org/10.1029/2019JD031224, 2019.

Cui, X., Wang, X., Yang, L., Chen, B., Chen, J., Andersson, A., and Gustafsson, Ö.: Radiative absorption

15   enhancement from coatings on black carbon aerosols, Sci. Total Environ., 551–552, 51–56, https://doi.org/10.1016/j.scitotenv.2016.02.026, 2016.

Dang, C., Segal-Rozenhaimer, M., Che, H., Zhang, L., Formenti, P., Taylor, J., Dobracki, A., Purdue, S., Wong, P.-S., Nenes, A., Sedlacek, A., Coe, H., Redemann, J., Zuidema, P., and Haywood, J.: Biomass burning and marine aerosol processing over the southeast Atlantic Ocean: A TEM single particle analysis, Atmospheric Chem. Phys.

20   Discuss., 1–30, https://doi.org/10.5194/acp-2021-724, 2021.

Feng, Y., Ramanathan, V., and Kotamarthi, V. R.: Brown carbon: a significant atmospheric absorber of solar radiation?, Atmospheric Chem. Phys., 13, 8607–8621, https://doi.org/10.5194/acp-13-8607-2013, 2013.

Formenti, P., Caquineau, S., Desboeufs, K., Klaver, A., Chevaillier, S., Journet, E., and Rajot, J. L.: Mapping the physico-chemical properties of mineral dust in western Africa: mineralogical composition, Atmospheric Chem.

25   Phys., 14, 10663–10686, https://doi.org/10.5194/acp-14-10663-2014, 2014.

Go, S., Lyapustin, A., Schuster, G. L., Choi, M., Ginoux, P., Chin, M., Kalashnikova, O., Dubovik, O., Kim, J., Silva, A. da, Holben, B., and Reid, J. S.: Inferring iron oxides species content in atmospheric mineral dust from DSCOVR EPIC observations, Atmospheric Chem. Phys. Discuss., https://doi.org/10.5194/acp-2021-599, 2021.

Gysel, M., Crosier, J., Topping, D. O., Whitehead, J. D., Bower, K. N., Cubison, M. J., Williams, P. I., Flynn, M.

30   J., McFiggans, G. B., and Coe, H.: Closure study between chemical composition and hygroscopic growth of aerosol particles during TORCH2, Atmospheric Chem. Phys., 7, 6131–6144, https://doi.org/10.5194/acp-7-6131-2007, 2007.

Hems, R. F., Schnitzler, E. G., Liu-Kang, C., Cappa, C. D., and Abbatt, J. P. D.: Aging of Atmospheric Brown Carbon Aerosol, ACS Earth Space Chem., 5, 722–748, https://doi.org/10.1021/acsearthspacechem.0c00346, 2021.

Ito, A., Lin, G., and Penner, J. E.: Radiative forcing by light-absorbing aerosols of pyrogenetic iron oxides, Sci. Rep., 8, 7347, https://doi.org/10.1038/s41598-018-25756-3, 2018.

5   Jacobson, M. Z.: Investigating cloud absorption effects: Global absorption properties of black carbon, tar balls, and soil dust in clouds and aerosols, J. Geophys. Res. Atmospheres, 117, https://doi.org/10.1029/2011JD017218, 2012.

Jo, D. S., Park, R. J., Lee, S., Kim, S.-W., and Zhang, X.: A global simulation of brown carbon: implications for photochemistry and direct radiative effect, Atmospheric Chem. Phys., 16, 3413–3432, 10   https://doi.org/10.5194/acp-16-3413-2016, 2016.

Kasthuriarachchi, N. Y., Rivellini, L.-H., Adam, M. G., and Lee, A. K. Y.: Light Absorbing Properties of Primary and Secondary Brown Carbon in a Tropical Urban Environment, Environ. Sci. Technol., 54, 10808–10819, https://doi.org/10.1021/acs.est.0c02414, 2020.

Kirchstetter, T. W. and Thatcher, T. L.: Contribution of organic carbon to wood smoke particulate matter 15   absorption of solar radiation, Atmospheric Chem. Phys., 12, 6067–6072, https://doi.org/10.5194/acp-12-6067-2012, 2012.

Kuang, Y., He, Y., Xu, W., Zhao, P., Cheng, Y., Zhao, G., Tao, J., Ma, N., Su, H., Zhang, Y., Sun, J., Cheng, P., Yang, W., Zhang, S., Wu, C., Sun, Y., and Zhao, C.: Distinct diurnal variation in organic aerosol hygroscopicity and its relationship with oxygenated organic aerosol, Atmospheric Chem. Phys., 20, 865–880, 20   https://doi.org/10.5194/acp-20-865-2020, 2020.

Kurisu, M., Adachi, K., Sakata, K., and Takahashi, Y.: Stable Isotope Ratios of Combustion Iron Produced by Evaporation in a Steel Plant, ACS Earth Space Chem., 3, 588–598, https://doi.org/10.1021/acsearthspacechem.8b00171, 2019.

Lack, D. A. and Cappa, C. D.: Impact of brown and clear carbon on light absorption enhancement, single scatter 25   albedo and absorption wavelength dependence of black carbon, Atmospheric Chem. Phys., 10, 4207–4220, https://doi.org/10.5194/acp-10-4207-2010, 2010.

Lack, D. A. and Langridge, J. M.: On the attribution of black and brown carbon light absorption using the Ångström exponent, Atmospheric Chem. Phys., 13, 10535–10543, https://doi.org/10.5194/acp-13-10535-2013, 2013.

30   Lack, D. A., Langridge, J. M., Bahreini, R., Cappa, C. D., Middlebrook, A. M., and Schwarz, J. P.: Brown carbon and internal mixing in biomass burning particles, Proc. Natl. Acad. Sci., 109, 14802–14807, https://doi.org/10.1073/pnas.1206575109, 2012.

Lamb, K. D., Matsui, H., Katich, J. M., Perring, A. E., Spackman, J. R., Weinzierl, B., Dollner, M., and Schwarz, J. P.: Global-scale constraints on light-absorbing anthropogenic iron oxide aerosols, Npj Clim. Atmospheric Sci., 4, 1–12, https://doi.org/10.1038/s41612-021-00171-0, 2021.

Laskin, A., Laskin, J., and Nizkorodov, S. A.: Chemistry of Atmospheric Brown Carbon, Chem. Rev., 115, 4335–4382, https://doi.org/10.1021/cr5006167, 2015.

Li, C., He, Q., Schade, J., Passig, J., Zimmermann, R., Meidan, D., Laskin, A., and Rudich, Y.: Dynamic changes in optical and chemical properties of tar ball aerosols by atmospheric photochemical aging, Atmospheric Chem. Phys., 19, 139–163, https://doi.org/10.5194/acp-19-139-2019, 2019.

Liati, A., Pandurangi, S. S., Boulouchos, K., Schreiber, D., and Arroyo Rojas Dasilva, Y.: Metal nanoparticles in diesel exhaust derived by in-cylinder melting of detached engine fragments, Atmos. Environ., 101, 34–40, https://doi.org/10.1016/j.atmosenv.2014.11.014, 2015.

Lin, P., Bluvshtein, N., Rudich, Y., Nizkorodov, S. A., Laskin, J., and Laskin, A.: Molecular Chemistry of Atmospheric Brown Carbon Inferred from a Nationwide Biomass Burning Event, Environ. Sci. Technol., 51, 11561–11570, https://doi.org/10.1021/acs.est.7b02276, 2017.

Liu, C., Chung, C. E., Yin, Y., and Schnaiter, M.: The absorption Ångström exponent of black carbon: from numerical aspects, Atmospheric Chem. Phys., 18, 6259–6273, https://doi.org/10.5194/acp-18-6259-2018, 2018.

Liu, D., Taylor, J. W., Young, D. E., Flynn, M. J., Coe, H., and Allan, J. D.: The effect of complex black carbon microphysics on the determination of the optical properties of brown carbon, Geophys. Res. Lett., 42, 613–619, https://doi.org/10.1002/2014GL062443, 2015.

Liu, D., Whitehead, J., Alfarra, M. R., Reyes-Villegas, E., Spracklen, D. V., Reddington, C. L., Kong, S., Williams, P. I., Ting, Y.-C., Haslett, S., Taylor, J. W., Flynn, M. J., Morgan, W. T., McFiggans, G., Coe, H., and Allan, J. D.: Black-carbon absorption enhancement in the atmosphere determined by particle mixing state, Nat. Geosci., 10, 184–188, https://doi.org/10.1038/ngeo2901, 2017.

Moteki, N., Kondo, Y., and Nakamura, S.: Method to measure refractive indices of small nonspherical particles: Application to black carbon particles, J. Aerosol Sci., 41, 513–521, https://doi.org/10.1016/j.jaerosci.2010.02.013, 2010.

Moteki, N., Adachi, K., Ohata, S., Yoshida, A., Harigaya, T., Koike, M., and Kondo, Y.: Anthropogenic iron oxide aerosols enhance atmospheric heating, Nat. Commun., 8, 15329, https://doi.org/10.1038/ncomms15329, 2017.

Palm, K. J., Murray, J. B., Narayan, T. C., and Munday, J. N.: Dynamic optical properties of metal hydrides, ACS Photonics, 5, 4677–4686, https://doi.org/10.1021/acsphotonics.8b01243, 2018.

Peng, J., Hu, M., Guo, S., Du, Z., Zheng, J., Shang, D., Levy Zamora, M., Zeng, L., Shao, M., Wu, Y.-S., Zheng, J., Wang, Y., Glen, C. R., Collins, D. R., Molina, M. J., and Zhang, R.: Markedly enhanced absorption and direct radiative forcing of black carbon under polluted urban environments, Proc. Natl. Acad. Sci., 113, 4266–4271, https://doi.org/10.1073/pnas.1602310113, 2016.

5 Pflüger, J. and Fink, J.: Handbook of Optical Constants of Solids, Academic Press, 293–310 pp., 1997.

Pistone, K., Redemann, J., Doherty, S., Zuidema, P., Burton, S., Cairns, B., Cochrane, S., Ferrare, R., Flynn, C., Freitag, S., Howell, S. G., Kacenelenbogen, M., LeBlanc, S., Liu, X., Schmidt, K. S., Sedlacek III, A. J., Segal-Rozenhaimer, M., Shinozuka, Y., Stamnes, S., van Diedenhoven, B., Van Harten, G., and Xu, F.: Intercomparison of biomass burning aerosol optical properties from in situ and remote-sensing instruments in ORACLES-2016, 10 Atmospheric Chem. Phys., 19, 9181–9208, https://doi.org/10.5194/acp-19-9181-2019, 2019.

Redemann, J., Wood, R., Zuidema, P., Doherty, S. J., Luna, B., LeBlanc, S. E., Diamond, M. S., Shinozuka, Y., Chang, I. Y., Ueyama, R., Pfister, L., Ryoo, J., Dobracki, A. N., da Silva, A. M., Longo, K. M., Kacenelenbogen, M. S., Flynn, C. J., Pistone, K., Knox, N. M., Piketh, S. J., Haywood, J. M., Formenti, P., Mallet, M., Stier, P., Ackerman, A. S., Bauer, S. E., Fridlind, A. M., Carmichael, G. R., Saide, P. E., Ferrada, G. A., Howell, S. G., 15 Freitag, S., Cairns, B., Holben, B. N., Knobelspiesse, K. D., Tanelli, S., L'Ecuyer, T. S., Dzambo, A. M., Sy, O. O., McFarquhar, G. M., Poellot, M. R., Gupta, S., O'Brien, J. R., Nenes, A., Kacarab, M. E., Wong, J. P. S., Small-Griswold, J. D., Thornhill, K. L., Noone, D., Podolske, J. R., Schmidt, K. S., Pilewskie, P., Chen, H., Cochrane, S. P., Sedlacek, A. J., Lang, T. J., Stith, E., Segal-Rozenhaimer, M., Ferrare, R. A., Burton, S. P., Hostetler, C. A., Diner, D. J., Platnick, S. E., Myers, J. S., Meyer, K. G., Spangenberg, D. A., Maring, H., and 20 Gao, L.: An overview of the ORACLES (ObseRvations of Aerosols above CLouds and their intEractionS) project: aerosol-cloud-radiation interactions in the Southeast Atlantic basin, Atmospheric Chem. Phys. Discuss., 1–82, https://doi.org/10.5194/acp-2020-449, 2020.

Saleh, R., Robinson, E. S., Tkacik, D. S., Ahern, A. T., Liu, S., Aiken, A. C., Sullivan, R. C., Presto, A. A., Dubey, M. K., Yokelson, R. J., Donahue, N. M., and Robinson, A. L.: Brownness of organics in aerosols from biomass 25 burning linked to their black carbon content, Nat. Geosci., 7, 647–650, https://doi.org/10.1038/ngeo2220, 2014.

Saleh, R., Marks, M., Heo, J., Adams, P. J., Donahue, N. M., and Robinson, A. L.: Contribution of brown carbon and lensing to the direct radiative effect of carbonaceous aerosols from biomass and biofuel burning emissions, J. Geophys. Res. Atmospheres, 120, 10,285-10,296, https://doi.org/10.1002/2015JD023697, 2015.

Sedlacek III, A. J., Buseck, P. R., Adachi, K., Onasch, T. B., Springston, S. R., and Kleinman, L.: Formation and 30 evolution of tar balls from northwestern US wildfires, Atmospheric Chem. Phys., 18, 11289–11301, https://doi.org/10.5194/acp-18-11289-2018, 2018.

Taylor, J. W., Wu, H., Szpek, K., Bower, K., Crawford, I., Flynn, M. J., Williams, P. I., Dorsey, J., Langridge, J. M., Cotterell, M. I., Fox, C., Davies, N. W., Haywood, J. M., and Coe, H.: Absorption closure in highly aged biomass burning smoke, Atmospheric Chem. Phys., https://doi.org/10.5194/acp-2020-333, 2020.

Till, J. L., Guyodo, Y., Lagroix, F., Morin, G., and Ona-Nguema, G.: Goethite as a potential source of magnetic nanoparticles in sediments, Geology, 43, 75–78, https://doi.org/10.1130/G36186.1, 2015.

Virkkula, A.: Correction of the Calibration of the 3-wavelength Particle Soot Absorption Photometer (3λ PSAP), Aerosol Sci. Technol., 44, 706–712, https://doi.org/10.1080/02786826.2010.482110, 2010.

5   Wang, J., Nie, W., Cheng, Y., Shen, Y., Chi, X., Wang, J., Huang, X., Xie, Y., Sun, P., Xu, Z., Qi, X., Su, H., and Ding, A.: Light absorption of brown carbon in eastern China based on 3-year multi-wavelength aerosol optical property observations and an improved absorption Ångström exponent segregation method, Atmospheric Chem. Phys., 18, 9061–9074, https://doi.org/10.5194/acp-18-9061-2018, 2018a.

Wang, L., Li, Z., Tian, Q., Ma, Y., Zhang, F., Zhang, Y., Li, D., Li, K., and Li, L.: Estimate of aerosol absorbing components of black carbon, brown carbon, and dust from ground-based remote sensing data of sun-sky

10   radiometers, J. Geophys. Res. Atmospheres, 118, 6534–6543, https://doi.org/10.1002/jgrd.50356, 2013.

Wang, X., Heald, C. L., Sedlacek, A. J., de Sá, S. S., Martin, S. T., Alexander, M. L., Watson, T. B., Aiken, A. C., Springston, S. R., and Artaxo, P.: Deriving brown carbon from multiwavelength absorption measurements: method and application to AERONET and Aethalometer observations, Atmospheric Chem. Phys., 16, 12733–

15   12752, https://doi.org/10.5194/acp-16-12733-2016, 2016.

Wang, X., Heald, C. L., Liu, J., Weber, R. J., Campuzano-Jost, P., Jimenez, J. L., Schwarz, J. P., and Perring, A. E.: Exploring the observational constraints on the simulation of brown carbon, Atmospheric Chem. Phys., 18, 635–653, https://doi.org/10.5194/acp-18-635-2018, 2018b.

van der Werf, G. R., Randerson, J. T., Giglio, L., Collatz, G. J., Mu, M., Kasibhatla, P. S., Morton, D. C., DeFries,

20   R. S., Jin, Y., and van Leeuwen, T. T.: Global fire emissions and the contribution of deforestation, savanna, forest, agricultural, and peat fires (1997–2009), Atmospheric Chem. Phys., 10, 11707–11735, https://doi.org/10.5194/acp-10-11707-2010, 2010.

Wong, J. P. S., Tsagkaraki, M., Tsiodra, I., Mihalopoulos, N., Violaki, K., Kanakidou, M., Sciare, J., Nenes, A., and Weber, R. J.: Atmospheric evolution of molecular-weight-separated brown carbon from biomass burning,

25   Atmospheric Chem. Phys., 19, 7319–7334, https://doi.org/10.5194/acp-19-7319-2019, 2019.

Yoshida, A., Moteki, N., Ohata, S., Mori, T., Tada, R., Dagsson-Waldhauserová, P., and Kondo, Y.: Detection of light-absorbing iron oxide particles using a modified single-particle soot photometer, Aerosol Sci. Technol., 50, 1–4, https://doi.org/10.1080/02786826.2016.1146402, 2016.

Zhang, X. L., Wu, G. J., Zhang, C. L., Xu, T. L., and Zhou, Q. Q.: What is the real role of iron oxides in the

30   optical properties of dust aerosols?, Atmospheric Chem. Phys., 15, 12159–12177, https://doi.org/10.5194/acp-15-12159-2015, 2015.